Supplementary Figures

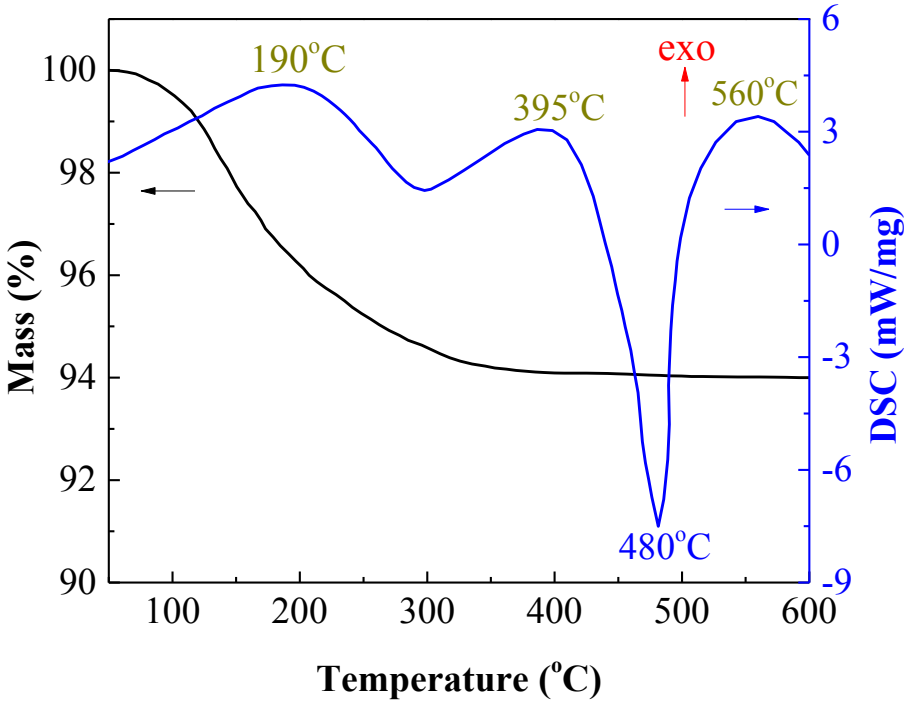

Figure 1. TG-DSC curve of the sample heated in argon from 50 to 600°C at a heating rate of 10°C/min.

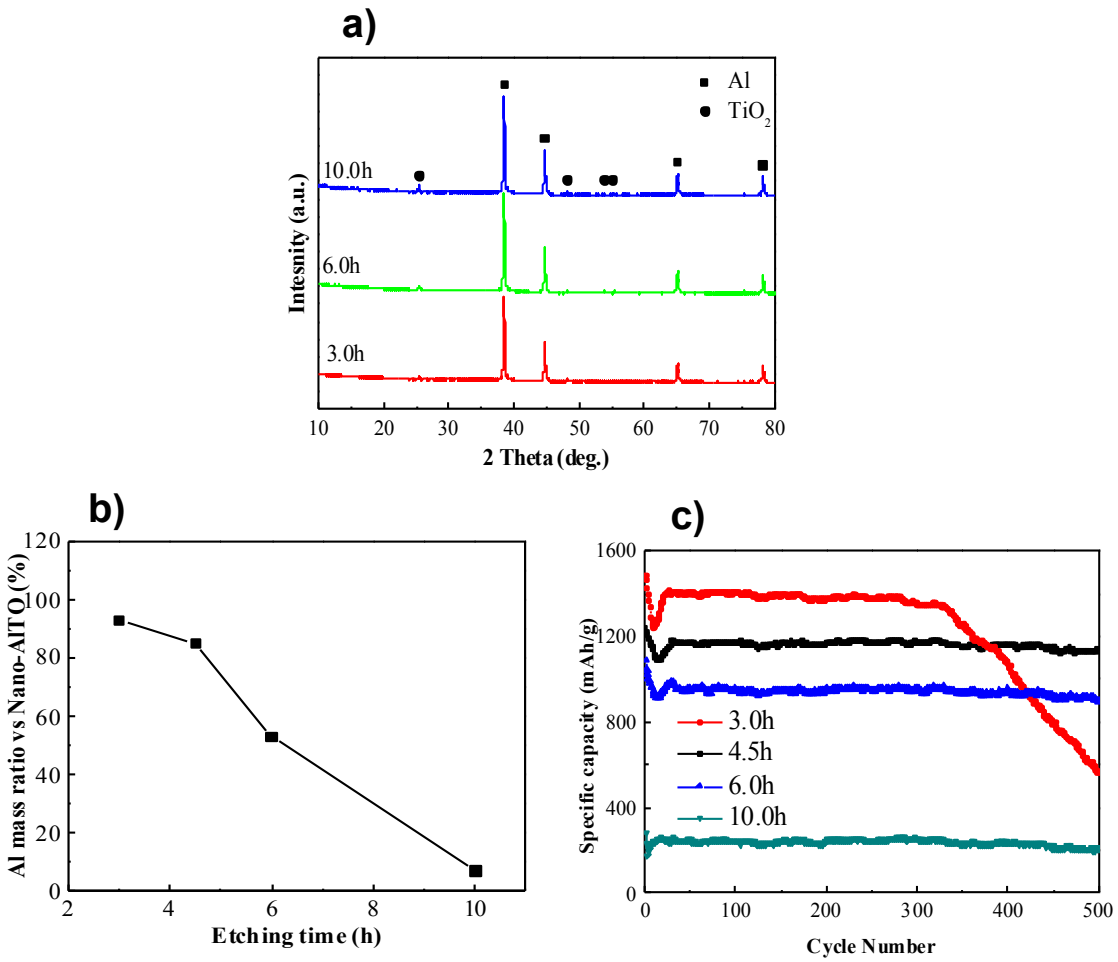

Figure 2. XRD and related battery performance of the etching time ranging 3.0 to 10.0 h. a) XRD patterns of the obtained Al@TiO_2. The crystal peaks indicate that the alumina was completely removed and a crystal TiO_2 was formed, as well as the sample with 4.5 h etching in Figure 1b. b) ICP results for Al weight ratio of samples with different etching time. c) Cycling life at 1 C. 3.0 h etching time shows rapid decay after 350 cycles since the voids are not sufficient enough.

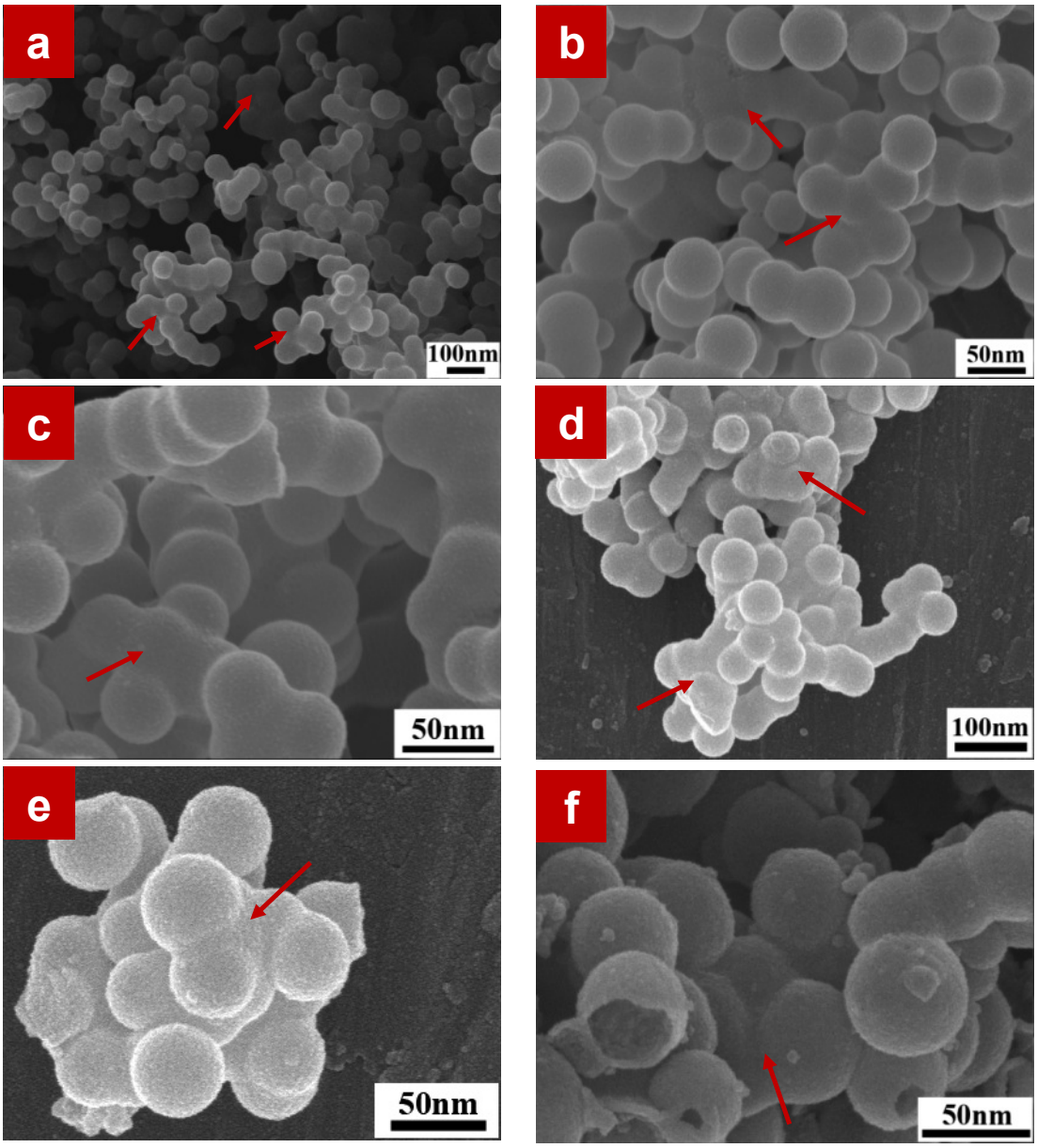

Figure 3. SEM images of as-obtained Al@TiO_2 with etching time of 4.5 h.

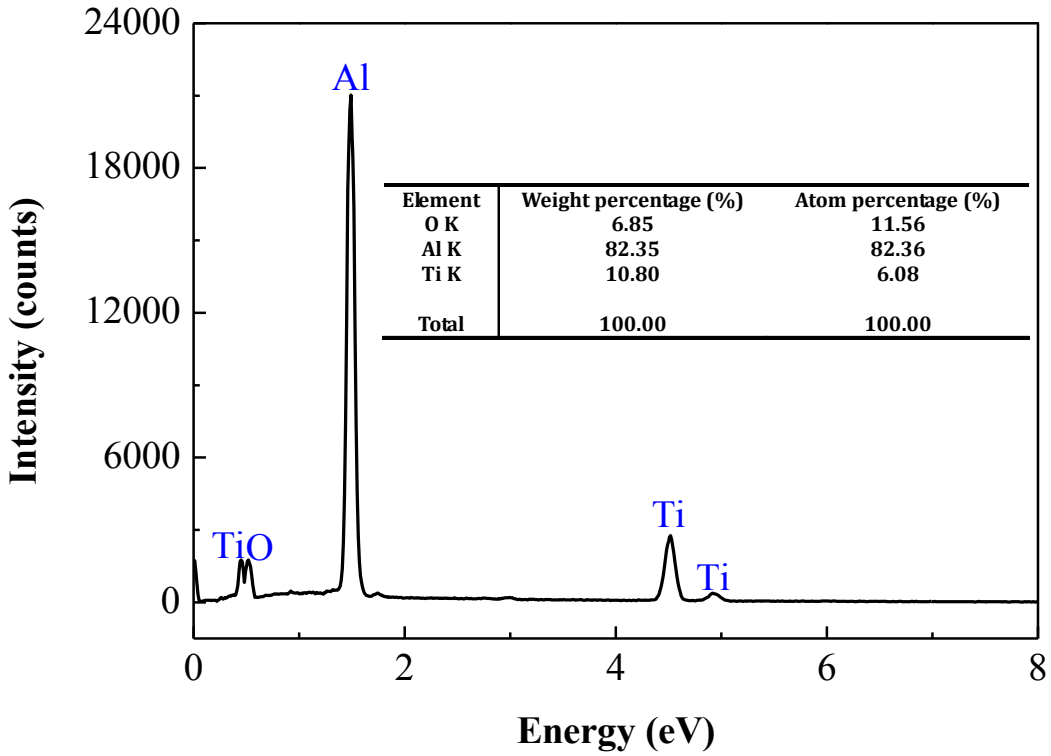

Figure 4. Energy-dispersive X-ray spectrum of the nanostructure in Figure S3a. The inset table shows that the weight fraction of Al is > 80 %.

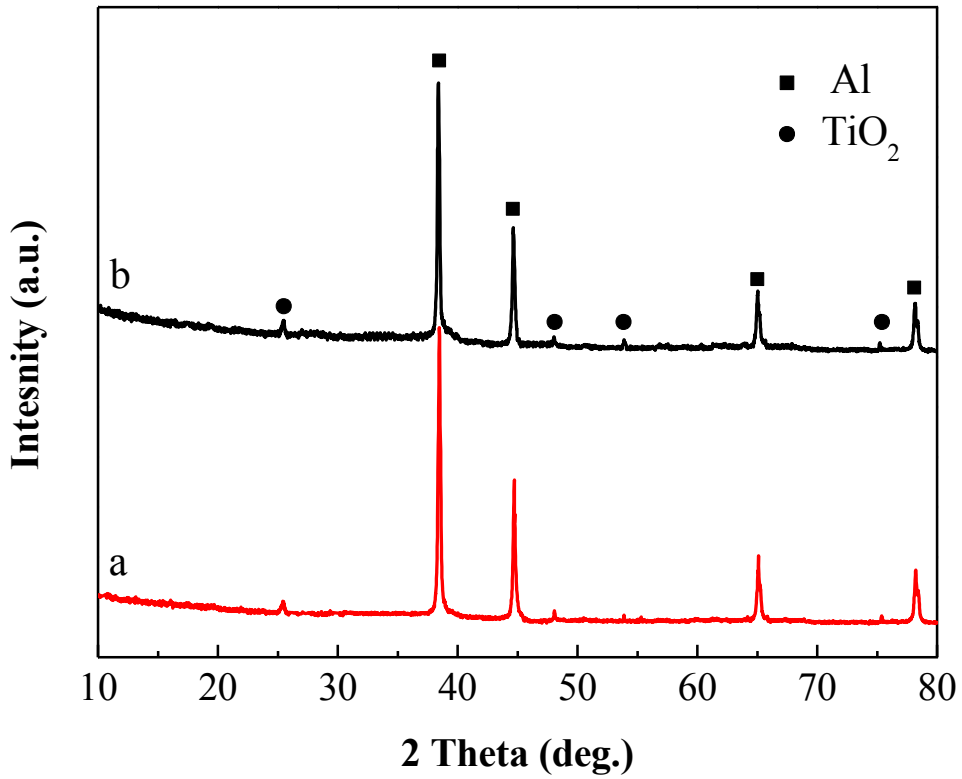

Figure 5. XRD characterization of Al@TiO_2 yolk-shell powders: a) exposed to ambient atmosphere for 24.0 h, b) grinded in air for 20 min (as we did when we prepared the electrodes, but handled without the conductive carbon black or poly(vinylidene fluoride) binder for simplicity of analysis) followed by exposing to air for another 24.0 h. No alumina peaks could be detected in both cases, which indicate negligible oxidation of aluminum core occurs.

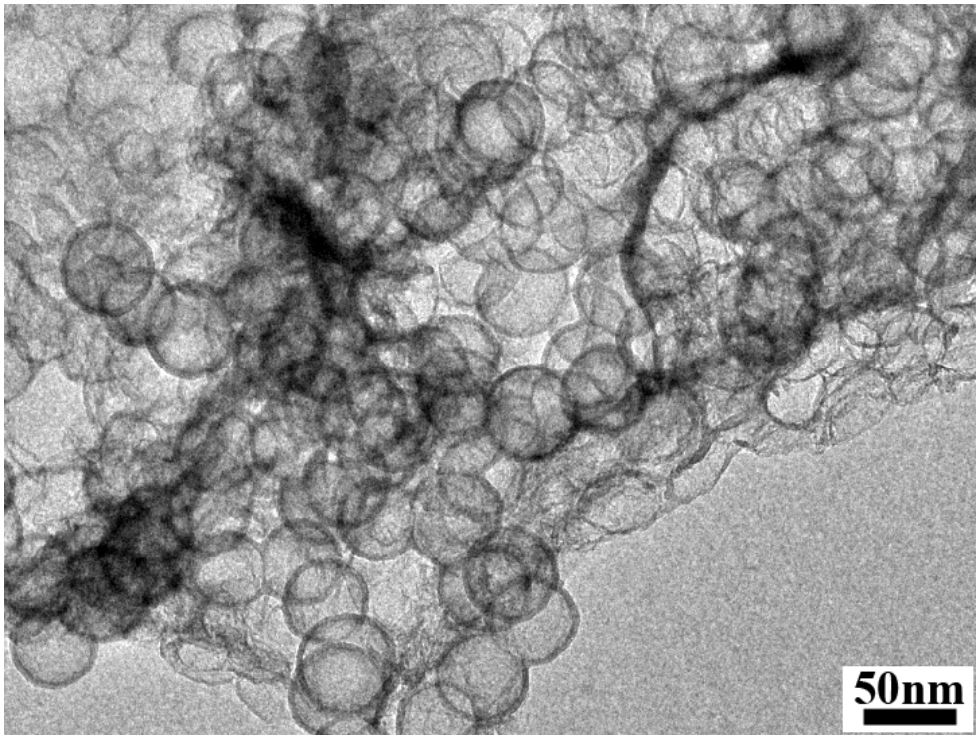

Figure 6. TEM image of the hollow TiO_2 (without Al) prepared using the etching time of 24 h. The obvious contrast between the edge and the center also reveals its hollow nature.

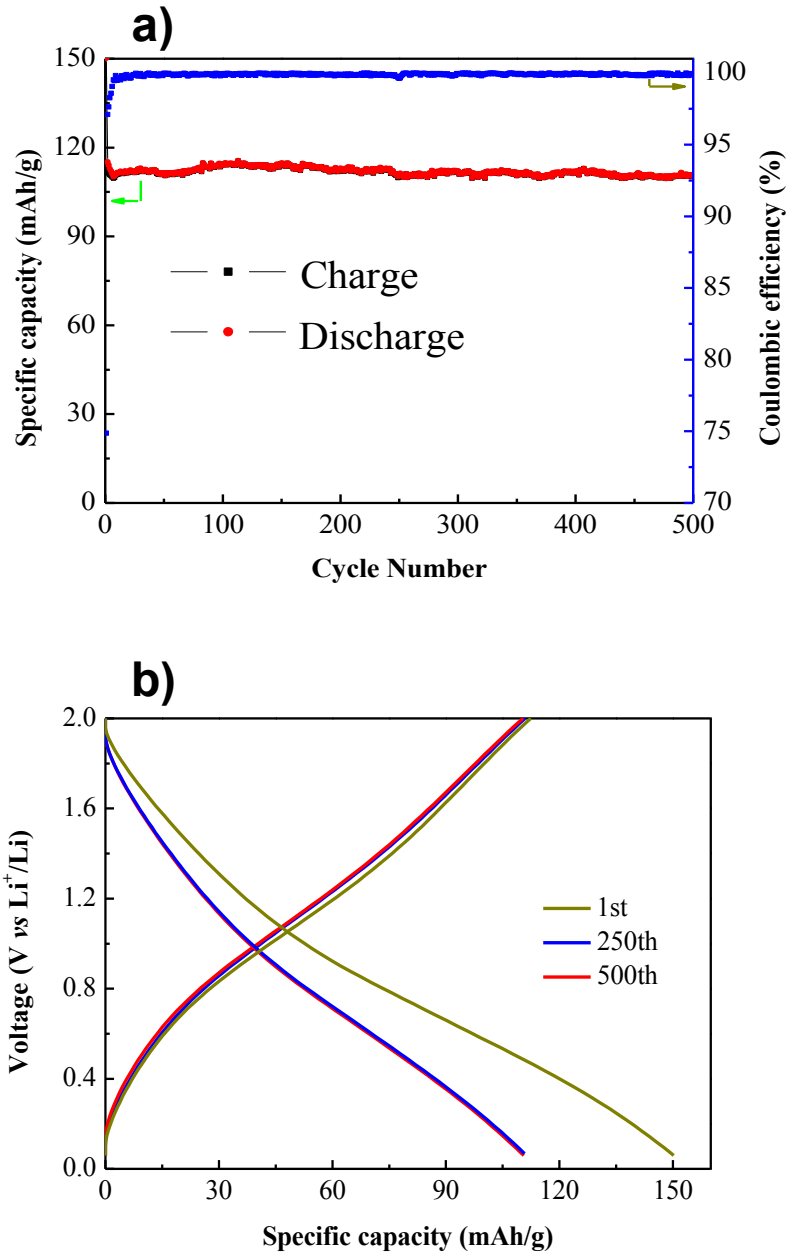

Figure 7. Battery performance of coin cells using TiO_2 hollow particles as cathode and Li foil as anode. a) Cycling life and the corresponding Coulombic efficiency during 500 cycles. The charge/discharge rate was set at 1 C. b) Charge/discharge voltage profiles with the 1st, 250th and 500th cycling.

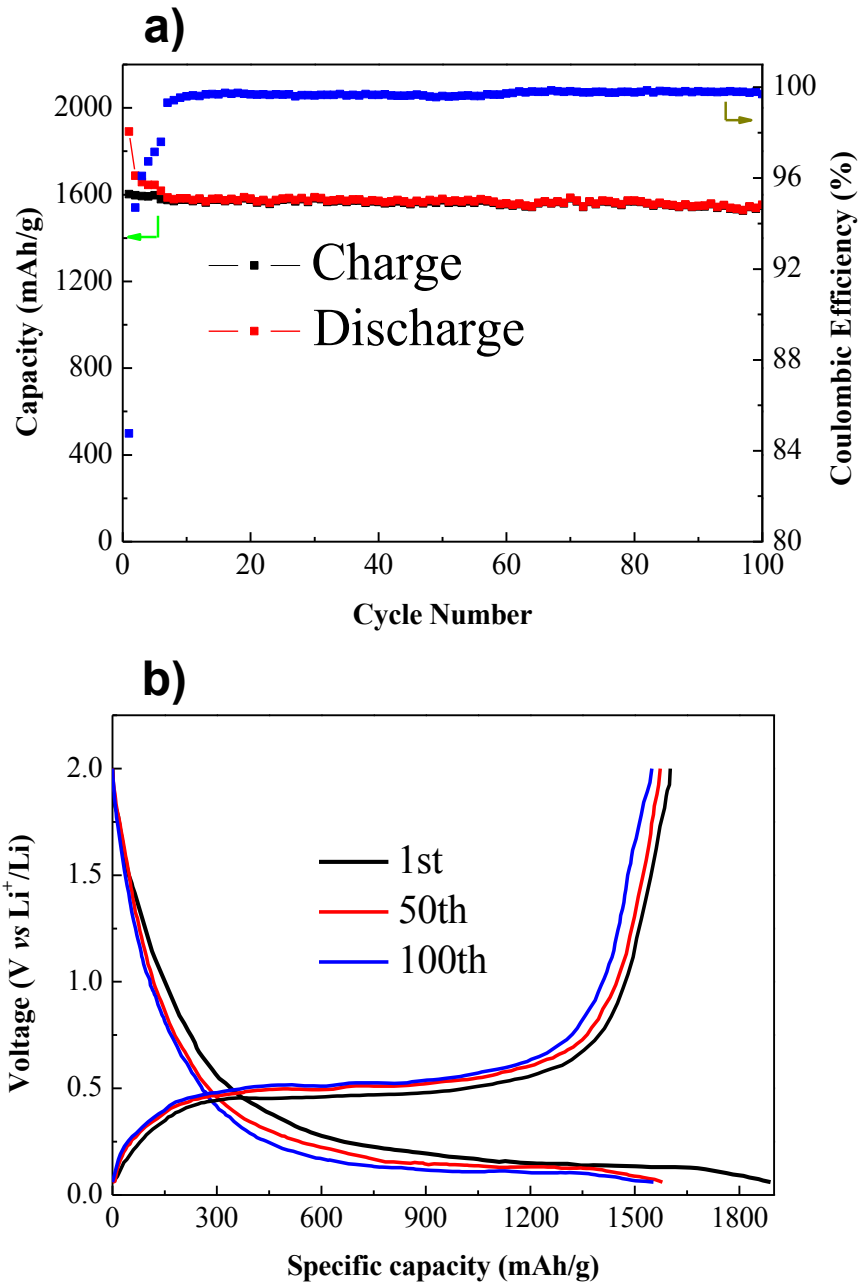

Figure 8. Battery performance of coin cells using Al@TiO_2 (4.5 h etching) as cathode and Li foil as anode. a) Cycling life and the corresponding Coulombic efficiency during 500 cycles. The charge/discharge rate was set at 0.1 C. b) Charge/discharge voltage profiles with the 1st, 50th and 100th cycling.

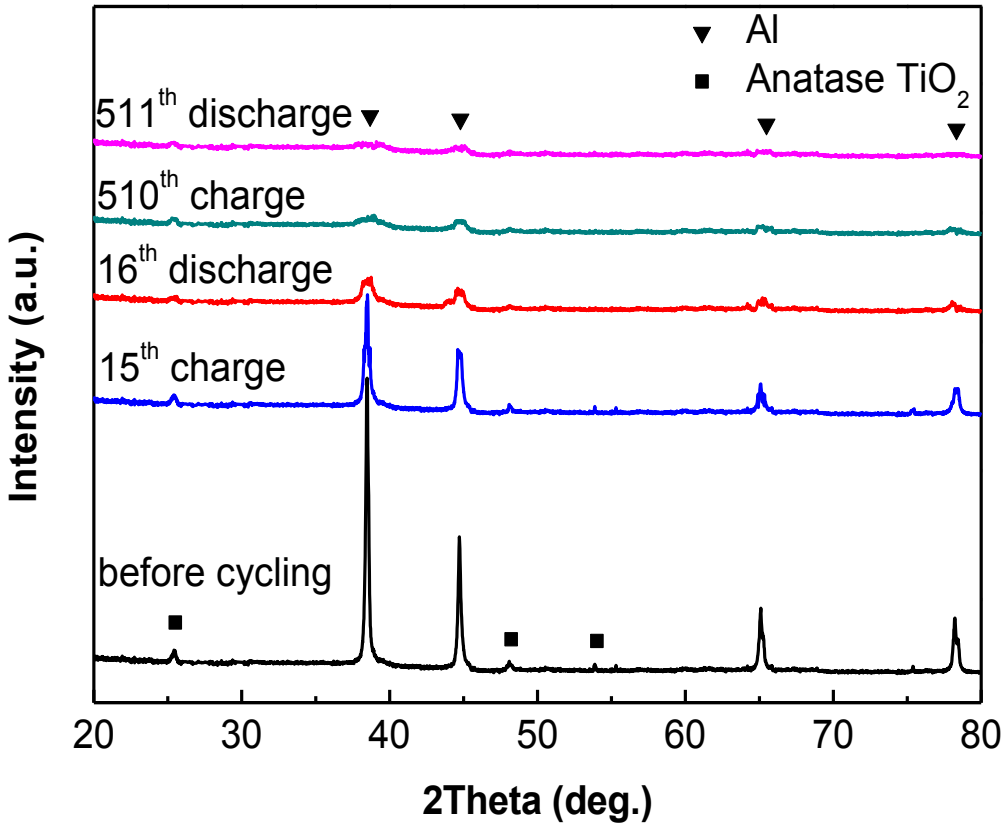

Figure 9. XRD pattern of Al@TiO_2 anode after cycling. As cycling increases, the Al FCC diffraction peaks at 38°, 44°, 65° and 78° decrease, which indicates the aluminum inside likely has turned amorphous.

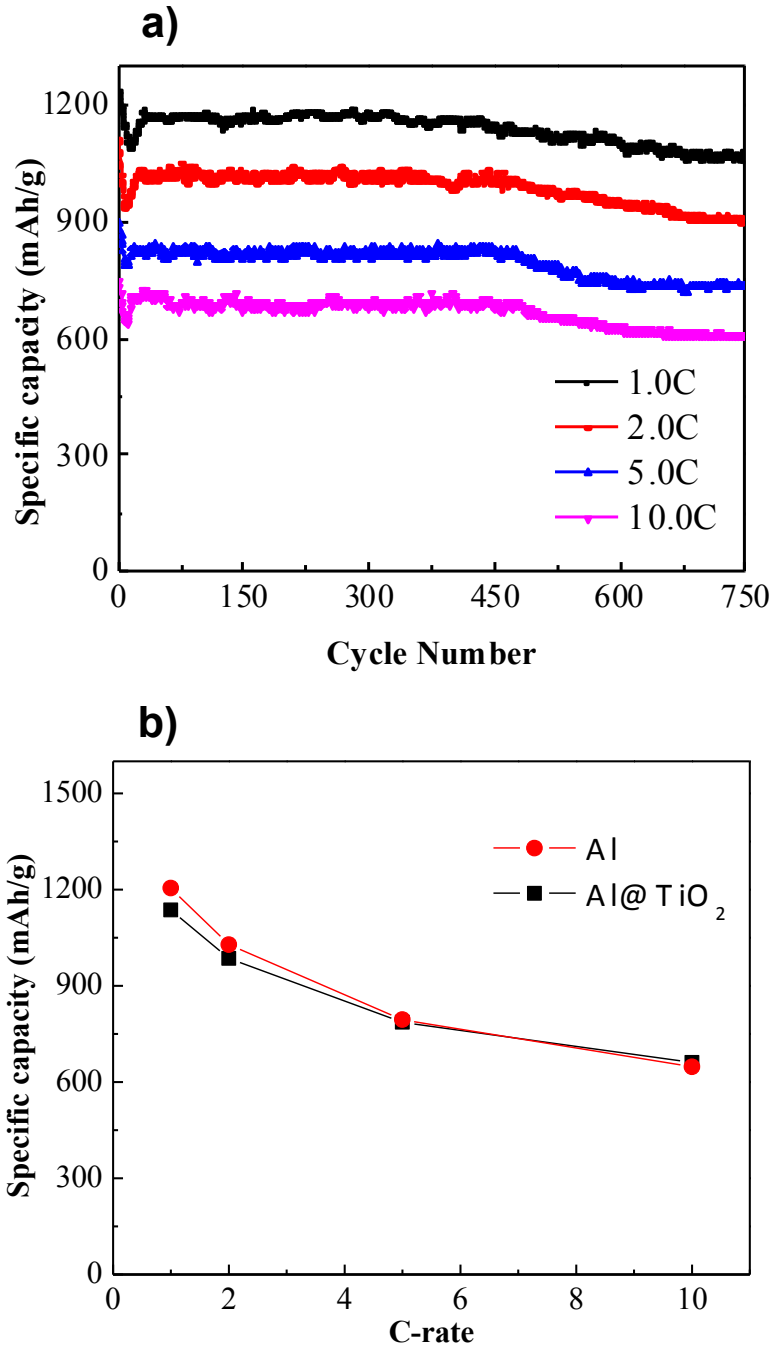

Figure 10. Battery performance of coin cells using 4.5 h etched Al@TiO_2 as anode and Li foil as cathode. a) Cyclability test at different charge/discharge rates during 750 cycles. b) The specific capacity was calculated at different charge/discharge rates according to the mass of pure aluminum.

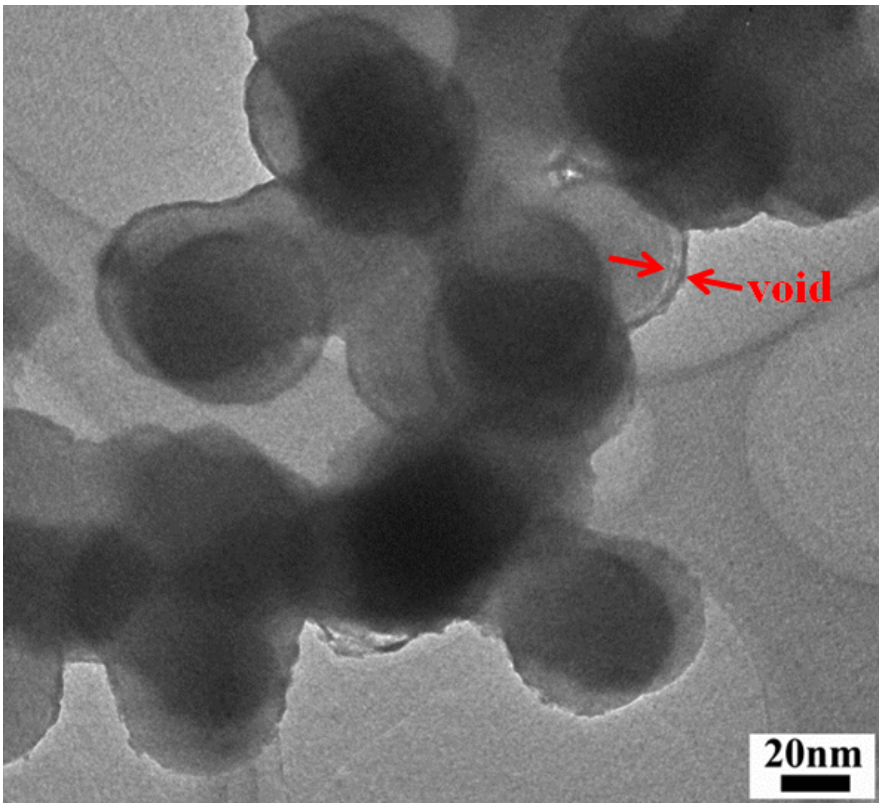

Figure 11. A TEM image of 3.0 h etched Al@TiO_2 after 450°C annealing with 1.0 h.

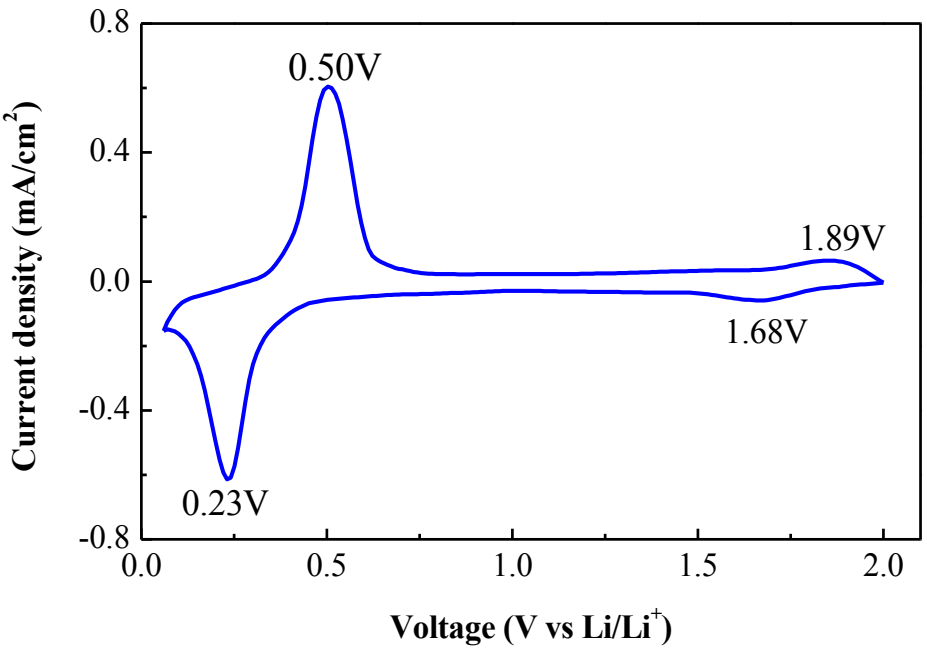

Figure 12. Cyclic voltammetry curve of an ATO/Li half-cell at 0.1 mV/s.

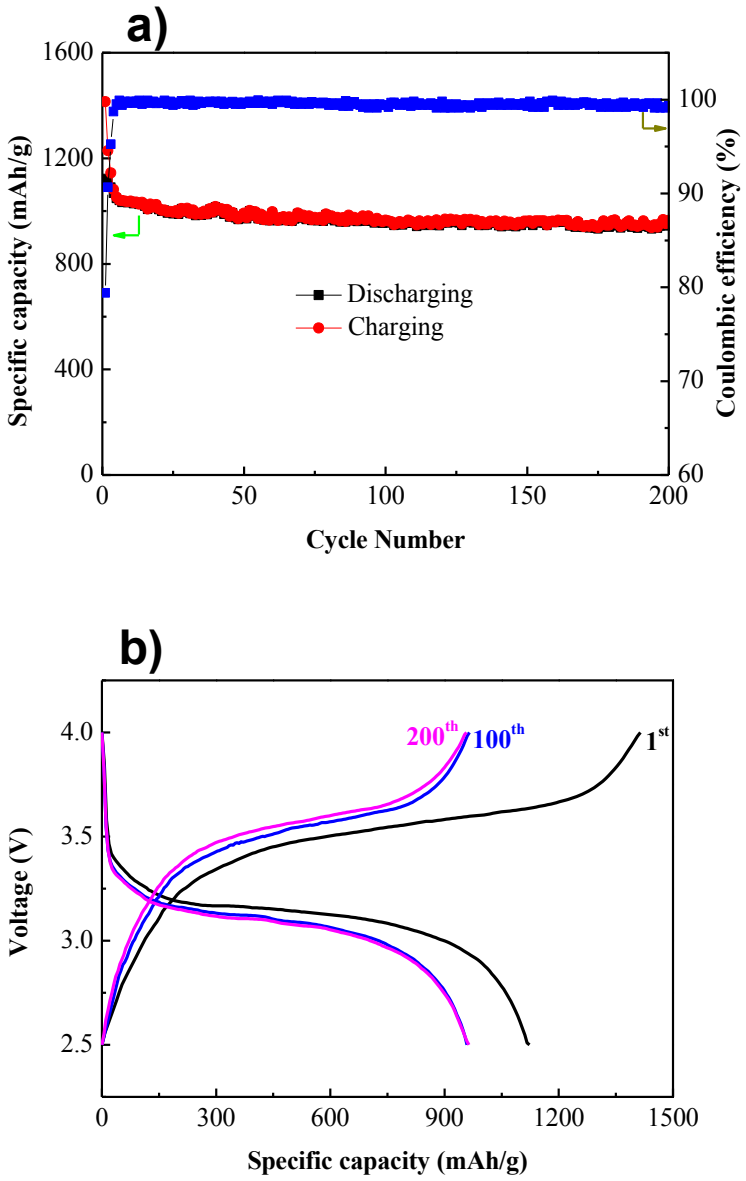

Figure 13. Battery performance of lithium-matched ATO/1M $LiPF_6$ EC:DEC/LFP full cells with only ~50% excess total lithium in the entire cathode and electrolyte salt compared to ATO capacity. a) Cycling life and the corresponding Coulombic efficiency during 200 cycles. The matched LFP/ATO full cells were cycled at 2.5-4.0 V, 1 C-rate (1410 mA g^{-1} of ATO). b) Charge/discharge voltage profiles with the 1st, 100th and 200th cycling.

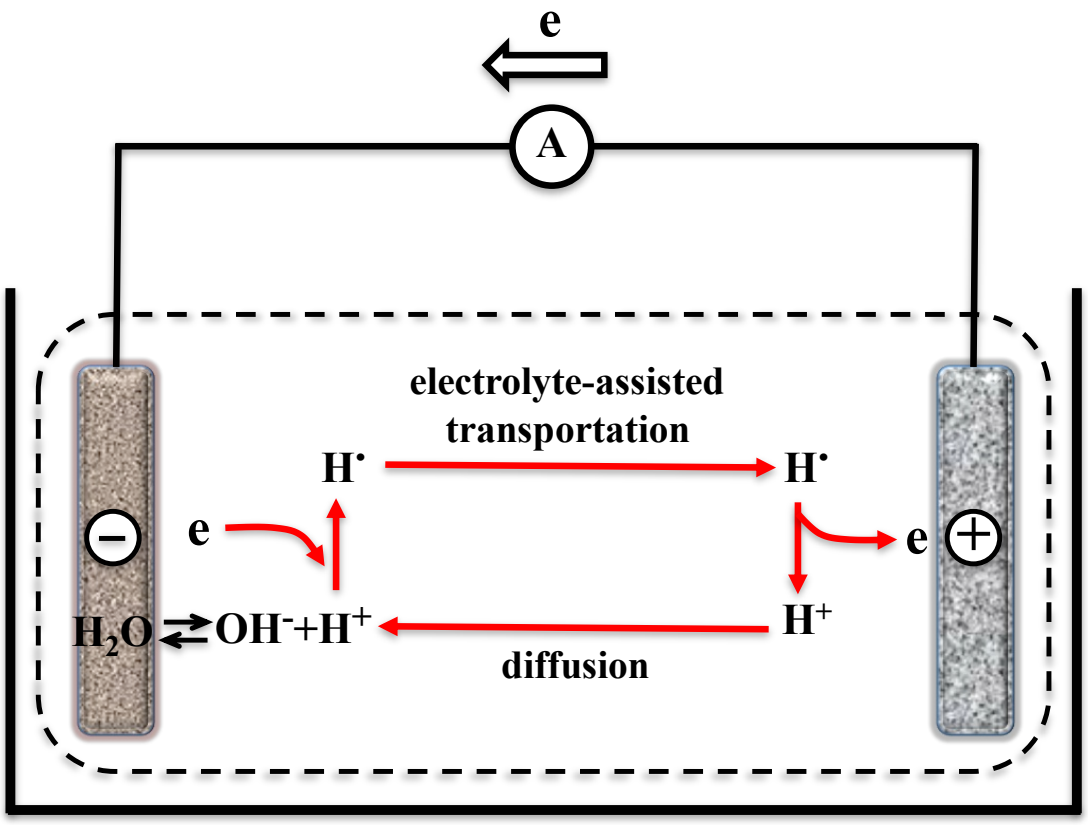

Figure 14. A possible mechanism of reversible water-related redox shuttle inside the electrolyte. (Adapted based on Fig.1 of Zhang, L., Zhang, Z.-C. & Amine, K. "Redox Shuttle Additives for Lithium-Ion Battery", in *Lithium Ion Batteries - New Developments* (ed Ilias Belharouak) (InTech, 2012).)

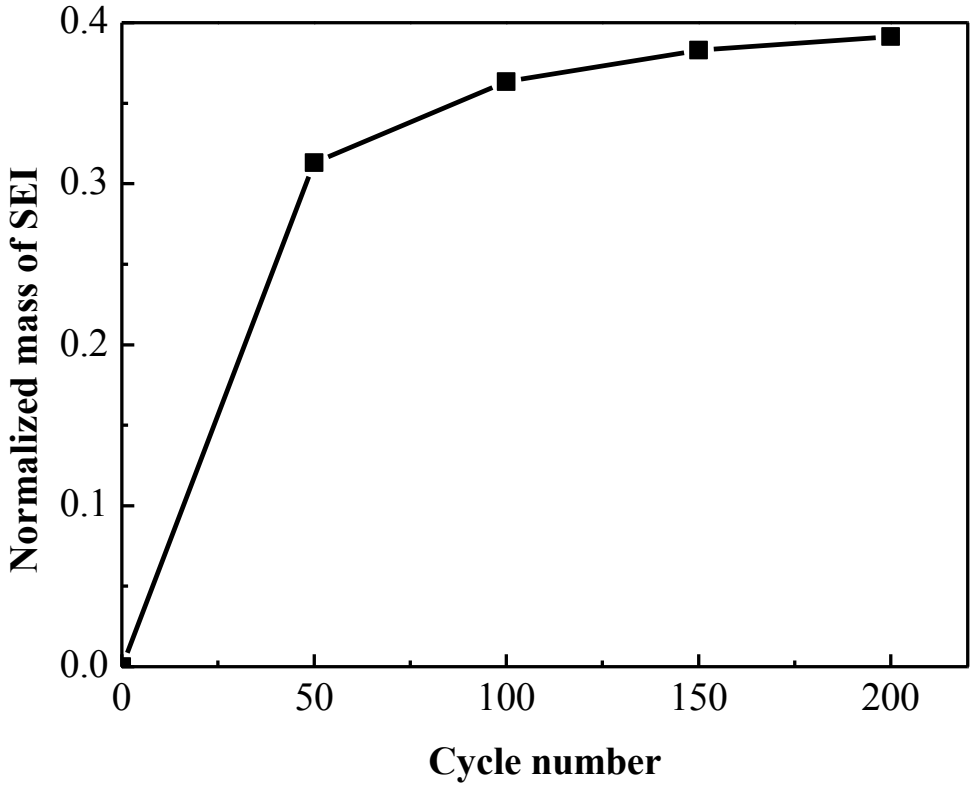

Figure 15. Mass gain of SEI on ATO in lithium-matched ATO/1M $LiPF_6$ EC:DEC/LFP full cells after 50, 100, 150 and 200 cycles, relative to the initial ATO weight (without binder and carbon black). Two LFP/ATO full cells were used for the average for each cycling condition.

Supplementary Table

Table 1. Comparison of battery performance of aluminum as anode in Li-ion batteries (The capacity was calculated based on the mass of aluminum).

1st discharge capacity (mAh/g)	Reversible discharge capacity (mAh/g)	Charge/discharge rate (A/g)	Total cycle number	Degradation rate per cycle	Potential range (*vs* Li^+/Li)	Ref.
1680	922 (100^{th})	6.0	100	0.60%	0.01-3 V	1
1200	100 (10^{th})	0.7	10	22.00%	0.01-3 V	2
1390	800 (1^{st})	0.25	1	42.40%	0.01-1.2 V	3
977	<200 (25^{th})	~1.0	25	>6.0%	0.01-1 V	4
1468	**1246 (500^{th})**	**1.4**	**500**	**0.01%**	**0.06-2 V**	**Current work**
	1205 (750^{th})	**(1.0 C vs Al_2Li_3)**	**750**	**0.03%**		

Supplementary Notes

To select an appropriate annealing temperature for Al@TiO_2, TG-DSC analysis was carried out, as shown in Supplementary Fig. 1. First the sample went through a dehydration process, displaying a loss of ~6 wt% at 100-300°C. Then a negligible weight loss was observed along with two exothermic and one endothermic peaks, which correspond to amorphous to anatase (395°C), anatase to rutile (560°C) TiO_2 phase transformation, and aluminum melting (480°C), respectively. For the purpose of obtaining crystal anatase TiO_2, we chose 450°C as the optimized annealing temperature in this study.

Supplementary Fig. 2a shows XRD patterns of Al@TiO_2 with etching time of 3.0, 6.0 and 10.0 h. It can be seen that the final product only consisted of pure aluminum and anatase TiO_2. Apparently the native Al_2O_3 layer was fully replaced by TiO_2 at different reaction time from 3.0 to 10.0 h. The reaction time mainly affects the size of interstitial space via dissolving the aluminum core. Supplementary Fig. 2b shows the aluminum concentration dependence on etching time. A shorter 3.0 h treatment enables a high aluminum concentration of >93 wt%, which indicates a small interspace (Supplementary Fig. 11). The interspace volume is estimated to be ~30% of the aluminum core, which is not enough to accommodate aluminum's ~96% volume expansion in lithiation. As a result, the TiO_2 shell was possibly damaged and thus a fast capacity decay happened (Supplementary Fig. 2c, red). A longer etching introduces a bigger interspace, which leads to better accommodation and then a good cyclability (Supplementary Fig. 2c). However, a lower aluminum ratio (~53 wt% with 6.0 h and ~7 wt% with 10.0 h) will introduce a lower specific capacity, which was calculated upon the total mass of Al@TiO_2 (Supplementary Fig. 2b). In parallel, larger interspace will reduce conductivity because of the loose contact, leading to higher impedance. The Al@TiO_2s treated with 6.0 and 10.0 h only show a specific capacity of ~903 and ~209 mAh/g after 500 cycles, respectively (Supplementary Fig. 2c). In conclusion, the sample of ~85 wt% Al with 4.5 h etching was selected to possess a near-optimal battery performance.

Supplementary Fig. 3 shows the double-yolk-single-shell or even multiple-yolk-single-shell structures caused by insufficient sonication and nanoparticle dispersal in acid. Energy-dispersive X-ray spectrum (Supplementary Fig. 4) of the nanostructure in Supplementary Fig. 3a demonstrates the presence of Al and TiO_2. The inset table shows that the weight fraction of Al is >80 %, which is also consistent with our ICP result in Supplementary Fig. 2b.

As we mentioned in the requirements of Al@TiO_2 yolk-shell nanostructures, the shell must be mechanically robust and fully closed. We believe our TiO_2 shell could semi-effectively protect the Al core. To verify this speculation, we did the XRD characterization of Al@TiO_2 yolk-shell powders that were exposed to ambient air for 24 h and grinded in air for 20 min (as we did when we prepared the electrodes, but handled without the conductive carbon black or poly(vinylidene fluoride) binder for simplicity of analysis) followed by exposing to air for

another 24 h. As revealed in Supplementary Fig. 5, no alumina peaks could be detected in both cases, which indicate negligible oxidation of aluminum core have occurred. Therefore, it is reasonable to conclude that Al@TiO_2 yolk-shell nanostructures are air stable for at least 24 h and the TiO_2 shell is mechanically robust to survive the mixing and handling during the electrode preparation.

The hollow TiO_2 (without Al) was obtained using an etching time of 24 h and the obvious contrast between the edge and the center in Supplementary Fig. 6 confirmed its hollow nature. The battery performance of the hollow TiO_2 shells was characterized, as shown in Supplementary Fig. 7. The reversible capacity reaches 112 mAh/g for the first cycle and stabilizes at 111 mAh/g for later cycles at a rate of 1 C. The average Coulombic efficiency is about 99.83% in the whole 500 cycles. The high reversibility also indicates the pseudocapacitive nature of the hollow TiO_2 shells.

The cycle performance at a slow rate of 0.1C was characterized for 100 cycles (Supplementary Fig. 8). The reversible capacity reaches 1638 mAh/g for the first cycle and stabilizes at 1599 mAh/g for later cycles at a rate of 0.1 C. The average Coulombic efficiency is about 99.41% in the first 100 cycles.

Supplementary Fig. 9 shows the XRD pattern of Al@TiO_2 anode after cycle. With increasing cycles, the Al FCC diffraction peaks at 38^o, 44^o, 65^o and 78^o decreases, which indicate the aluminum inside likely has turned amorphous.

In regards to aluminum as the active material, for a comparison, the specific capacity of Al@TiO_2 battery vs pure aluminum with different cycles and rates were also calculated. As shown in Supplementary Fig. 10b, the specific capacity of 1205 (1 C), 1028 (2 C), 795 (5 C), and 647 mAh/g (10 C) after 500 cycles was respectively attained, which further indicates the outstanding battery performance of the ATO electrode.

In our half-cell experiments, the average CE from 1^{st} to 500^{th} cycle is calculated to be 99.2%. However the 0.8% AWOL electrons are not all generating irreversible SEI, but we believe forming reversible redox shuttle inside the electrolyte, as illustrated in Supplementary Fig. 14. We have proposed it is water related. When there is a little bit of residual water in the electrode, which is reasonable in our situation considering that we prepare the electrodes in a moisture-containing environment, the redox shuttle mechanism may be activated between the Al@TiO_2 (ATO) cathode and lithium anode. During discharging, the absorbed water would firstly receive electrons ($H_2O+e^- \rightarrow H^{\bullet}+OH^-$), producing hydrogen radical ($H^{\bullet}$). Then the active hydrogen would preferably attach to the organic electrolyte, ethylene carbonate ($(CH_2O)_2CO$), for example, with the lone pair of the oxygen atom of carbonyl group in the EC interacting with the unsaturated hydrogen radical.

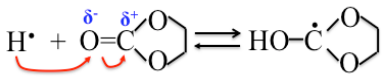

(1)

In this form, the hydrogen radical is protected from intermolecular annihilation and thus stabilized to survive the diffusion circle. Once the $H^{\bullet}$ is translated to the lithium metal, it would release the electron to form H^{+} again ($H^{\bullet} \rightarrow H^{+} + e^{-}$), which would diffuse back to the Al@TiO_2 electrode. The "oxidation-diffusion-reduction-diffusion" cycle can be repeated continuously due to the reversible nature of the redox shuttle. We did an estimation based on the Faraday's law. When the water fraction reaches 0.2% of the active materials, the Coulombic efficiency loss that comes from the residual water approaches 0.5%.

Supplementary Methods

Synthesis of Al@TiO_2 nanoparticles

Large quantities of Al@TiO_2 composites were synthesized through an "*in situ* water-shift" strategy (Figure 1a). In a typical experiment, we first prepare saturated titanium oxysulfate solution with 0.05 g $TiOSO_4$ (reagent grade, Sigma-Aldrich) and 3.0 g H_2SO_4 (ACS, 1N, VWR) dissolved in 100 mL DI water. Then 0.135 g commercial aluminum powders (99.9%, US Research Nanomaterials, Inc.), which showed an average diameter of ~50 nm in TEM images, were added to the saturated titanium oxysulfate solution. Then the mixture was sonicated with 30 min using an ultrasound cleaner (Symphony^{TM}, VMR). The obtained slurry was continuously stirred with 3.0-10.0 h afterwards until the color changed from grey to light. The resultant solution under different reaction time was then filtrated in a vacuum system and washed three times by ethanol. The received paste was dried at 70°C with 7.0 h in a vacuum oven (Symphony^{TM}, VMR). The dried sample was annealed at 450°C with 1.0 h in an Ar filled quartz tube furnace (Lindberg Blue M, Thermo Scientific). After cooling to room temperature, the sample was collected for the following characterization and battery test.

Characterization

XRD measurements were carried out via a Bruker D8-Advance diffractometer using Ni filtered Cu Kα radiation. The applied current and voltage were 40 mA and 40 kV, respectively. During the analysis, the sample was scanned from 10 to 70^o at a speed of 4^o/min. SEM images were collected on a FEI Sirion scanning electron microscope (accelerating voltage 5 kV) equipped with energy-dispersive X-ray spectroscopy and TEM images were taken on a JEOL JEM-2010 transmission electron microscope operated at 200 kV. TG-DSC analysis was performed using Netzsch STA 449 with air flow at a heating rate of 10°C/min from room temperature to 600°C. Inductively coupled plasma mass spectrometry (ICP-MS) was carried out using a Thermo Scientific ICAP 6300 Duo View Spectrometer.

To characterize the anode morphology evolution after cycling (Figure 4), the coin cell was opened after 500 cycles. The Al@TiO_2 anode was washed in acetonitrile to remove the electrolyte and rinsed with ethanol 3 times.

Electrochemical Test

The battery performance of Al@TiO_2 as anode was tested using a coin cell (CR2032, Panasonic). The working electrode was prepared by mixing Al@TiO_2 (70 wt%) with 15 wt% conductive carbon black (Super C65, Timcal), and 15 wt% poly(vinylidene fluoride) binder (average M_n ~71,000, Sigma-Aldrich) in N-methyl-2-pyrrolidinone (NMP, Sigma-Aldrich), which then was coated onto a copper foil with a loading of 3 mg/cm^2 of the Al@TiO_2 and dried at 65°C for 24.0 h in an oven (Symphony^{TM}, VMR). The coin cell using a lithium foil as counter electrode was assembled in a glove box (Labmaster sp, MBraun) filled with argon (both O_2 and

H_2O <0.1 ppm). To suppress lithium dendrite formation and also improve the cycle performance of the lithium foil in half-cell, a Li_3N passivation layer was coated on the lithium foil electrode before battery assembly. The pretreatment procedure exposes one face of a fresh Li foil (thickness ~600 μm) to flowing N_2 gas at a constant velocity for 2 h at room temperature to form Li_3N. When preparing the half-cell, the pretreated side of lithium foil would be in contact with the electrolyte. A hydraulic crimping machine (MSK-110, MTI) was used to pack the cell. The electrolyte was 1.0 M $LiPF_6$ dissolved in 1:1 volume ratio ethylene carbonate and diethyl carbonate, and a microporous polyethylene film (Celgard 2400) as the separator. Before use, the separator was soaked in the electrolyte overnight. The assembled cell was cycled in the fixed voltage window between 0.06 to 2.0 V at various rates ranging 0.1 to 10 C with an LAND 2001 CT battery tester. All of the specific capacities were calculated on the basis of the total mass of Al@TiO_2 except the data in Table S1 and Figure S6 were based on pure aluminum. The cyclic voltammetry curves were obtained at room temperature using the coin cells above between 0.06 and 2 V at a scan rate of 0.1 mV/s. Full cells consisting of ATO as the anode, $LiFePO_4$ (LFP) as the cathode, and a 1M $LiPF_6$ EC:DEC 1:1 solution as the electrolyte were fabricated and tested. The ATO anode was prepared using the same method described above and the electrode film was punched into discs with diameters of 10 mm before battery assembling in a glove box filled with argon gas. The LFP electrodes were fabricated by spreading the mixture of LFP (Pulead Technology Industry Co., Ltd.), carbon black (Super C65, Timcal) and poly(vinylidene fluoride) binder (Sigma-Aldrich) with a weight ratio of 80:10:10 onto Al current collectors. The electrode was pressed under 6-10 MPa and punched into 11 mm diameter circular disks. The active material loading was 1.3 mg/cm^2 for the ATO anode and 10.5 mg/cm^2 for the LFP cathode. The mass of ATO, LFP and even the Lithium salt in the electrolyte was carefully calculated/weighed, and the total lithium contained in our full cells does not exceed ~150% of the ATO capacity in half-cell. The matched ATO/LFP full cells were evaluated by galvanostatic cycling in a 2032 coin-type cell at 2.5-4.0 V, 1 C-rate (1410 mA g^{-1} of ATO). The mass of SEI layers is estimated by measuring the mass of ATO active materials based anode before and after 50, 100, 150 and 200 cycles. The normalized mass of SEI is defined as the ratio of the mass gain on ATO after cycling (presumably due to SEI layers covering ATO) to the initial ATO mass loaded in the cell without SEI. Two LFP/ATO full cells were used for the average normalized mass of SEI for each cycling condition.

Supplementary References

1 Park J H, Hudaya C, Kim A Y, et al. Al–C hybrid nanoclustered anodes for lithium ion batteries with high electrical capacity and cyclic stability. *Chem Commun* **50**, 2837-2840, (2014).

2 Au M, McWhorter S, Ajo H, et al. Free standing aluminum nanostructures as anodes for Li-ion rechargeable batteries. *J Power Sources* **195**, 3333-3337, (2010).

3 Hamon Y, Brousse T, Jousse F, et al. Aluminum negative electrode in lithium ion batteries. *J Power Sources* **97-8**, 185-187, (2001).

4 Hudak N, Huber D. Nanostructured Lithium-Aluminum Alloy Electrodes for Lithium-Ion Batteries. *ECS Transaction* **33**, 1-13 (2011)